Journal of Materials Chemistry A

ROYAL SOCIETY OF CHEMISTRY

PAPER

View Article Online
View Journal | View Issue

Cite this: J. Mater. Chem. A, 2020, 8, 14713

Highly permeable and selective mixed-matrix membranes for hydrogen separation containing PAF-1†

Rujing Hou, [a] Bader S. Ghanem,[b] Stefan J. D. Smith, [ac] Cara M. Doherty, [c] Caitlin Setter,[a] Huanting Wang, [a] Ingo Pinnau *[b] and Matthew R. Hill *[ac]

As the potential for a hydrogen economy re-emerges globally, its distribution is a key enabling capability to master. One option is to utilise the existing reticulated natural gas infrastructure, mixing in a minor component of hydrogen to form a composition commonly known as Hythane. After distribution, should the hydrogen be utilised within a fuel cell, it must be extracted from the Hythane mixture. Membranes offer the most efficient means of achieving such a separation, due to the lack of need for a phase change to occur. Sufficient selectivity within the membrane is required due to the relatively low (10–15%) composition of hydrogen within Hythane, and the very high purities required for fuel cell operation. Polymers of Intrinsic Microporosity (PIMs) are of interest for this application due to their innately high selectivity, albeit presently short of that required. Previously, we have shown that the porous framework PAF-1 can control physical aging within related systems. Here, we reveal that the use of a highly rigid ladder polymer, TPIM-2, can deliver a H_2/CH_4 selectivity as high as 16 in PAF-1 nanocomposites, which could reach 62.6 after aging. Encouragingly, the selectivity increase was also accompanied by a permeability enhancement, with as much as 4886 barrer recorded for hydrogen permeability. This favourable combination of hydrogen permeability and selectivity results in the aged MMMs surpassing the 2015 upper bound for H_2/CH_4 separation. Mechanistic investigations revealed that PAF-1 not only provided more gas transport channels for higher membrane permeability, but also accelerated the aging process leading to significantly improved membrane selectivity.

Received 18th May 2020
Accepted 3rd July 2020

DOI: 10.1039/d0ta05071g

rsc.li/materials-a

Introduction

Membrane-based gas separation technology has become a well-established method in industry due to the potential merits of lower operating- and capital cost, simple continuous operation and smaller footprint than conventional distillation, solid state adsorption or liquid phase absorption processes.[1–4] Hydrogen, for use as a clean energy fuel with the consideration of low carbon emission environmental regulations, requires purification that is most efficiently performed by a membrane separation.[5–7] Commercial membrane materials such as polyimide (PI), polycarbonate (PC), cellulose acetate (CA) and polysulfone (PSF), show favourable hydrogen selectivity (polysulfone, $H_2/N_2 = 56$, $H_2/CH_4 = 56$), but low permeabilities ($P(H_2) \sim 10$–20 barrer, where 1 barrer $= 1 \times 10^{-10}$ cm^3 (STP) cm cm^{-2} s^{-1} cmHg^{-1}), resulting in enormous membrane area and high system capital cost requirements.[8–10] To improve membrane permeability, and reduce system costs, several advanced high fractional free volume polymers have been developed, including polymers of intrinsic microporosity (PIMs), such as ladder PIM-1, and linear chain PTMSP.[11–14] Gas permeabilities in PIMs are often several orders of magnitude higher than traditional polymers; however the boost in permeability is usually coupled with a drop in selectivity, as first postulated by Robeson.[15] For instance, the archetypical PIM-1 has a hydrogen permeability $P(H_2)$ of 4900 barrer, but a selectivity over methane of just 4.8.[16] Since Robeson's observations, this trade-off between permeability and selectivity has been one of the most investigated challenges for membrane science and technology.[15,17] The unprecedented performance of more recently reported PIMs have mandated a shift in the upper bound curve for several gas pairs, including H_2/CH_4 and H_2/N_2, most recently in 2015 by Pinnau and co-workers.[18,19] One class of polymeric materials that demonstrated permselectivity performance near the 2015 upper bound curve for H_2/N_2 and H_2/CH_4, is based on phenazine-containing triptycene ladder polymers (TPIMs) made by AB polymerization.[20] Fine-tuning of the porous texture of the

[a]Department of Chemical Engineering, Monash University, Clayton, Victoria 3168, Australia. E-mail: matthew.hill@monash.edu

[b]Functional Polymer Membranes Group, Advanced Membranes and Porous Materials Center, Division of Physical Science and Engineering, King Abdullah University of Science and Technology, 23955, Thuwal, Saudi Arabia. E-mail: ingo.pinnau@kaust.edu.sa

[c]CSIRO, Bag 10, Clayton South, Victoria 3169, Australia. E-mail: Matthew.Hill@csiro.au

† Electronic supplementary information (ESI) available. See DOI: 10.1039/d0ta05071g

TPIMs was achieved by using branched alkyl (i-propyl – TPIM-1) or linear alkyl (*n*-propyl – TPIM-2) side groups in the 9,10-bridgehead position of the triptycene moiety. Previously, favourable hydrogen separation selectivity ($H_2/N_2 = 37$, $H_2/CH_4 = 36$) was recorded for TPIM-2 after 14 days storage under ambient conditions.[20] In sharp contrast, we reported a hydrogen selectivity of less than 10 for PIM-1 in our previous work ($H_2/N_2 = 7.5$, $H_2/CH_4 = 4.8$).[16] The enhanced hydrogen selectivity of TPIM-2 was accompanied with a reduction in H_2 permeability (655 barrer)[20] with respect to PIM-1 (4900 barrer).[16] However, relative to commercial low-free-volume glassy membrane materials, such as polysulfone, TPIM-2 exhibits a ~50-fold improvement in H_2 permeability.

In previous studies, we utilized PAF-1 as an additive in MMMs both for gas- and liquid separations and demonstrated that gas permeability in MMMs can be significantly increased without selectivity loss, and in some studies, resulted in MMM with anti-aging properties. For example, a PAF-1-containing thermally rearranged 6FDA-HAB-DAM mixed-matrix membrane showed 37-fold enhancement in H_2 permeability with similar gas-pair selectivity.[21] When PAF-1 was combined with PTMSP, PMP, or PIM-1, the resulting MMMs lost only 5–7% CO_2 permeability over 240 days rather than 38–62% permeability decrease observed for the pure polymer membranes.[14] In pervaporation studies, the inclusion of PAF-1 into PTMSP membranes resulted in a 31% increase of ethanol flux and 52% improvement of ethanol/water separation factor.[22]

In this work, mixed-matrix membranes were prepared by incorporating PAF-1 into TPIM-2 ladder polymer to enhance the gas separation performance. A series of characterization techniques, including scanning electron microscope (SEM), X-ray diffraction (XRD), Fourier-transform infrared spectroscopy (FT-IR), viscosity measurements, positronium annihilation lifetime spectroscopy (PALS), low temperature N_2 gas sorption for BET analysis and gas permeation studies were used to investigate the structural changes of the TPIM-2 matrix induced by the PAF-1 filler.

Experimental section

Materials

Reagents and solvents including bis(1,5-cyclooctadiene)nickel(0), 2,2′-bipyridyl, 1,5-cyclooctadiene, tetrakis(4-bromophenyl) methane, anhydrous dimethylformamide (DMF), calcium hydride (CaH_2), hydrochloric acid (HCl, 37%), anhydrous chloroform ($CHCl_3$), tetrahydrofuran (THF), deionized water (H_2O), veratrole, butyraldehyde, acetonitrile, sulfuric acid (H_2SO_4, 98%), methanol, acetone, silica gel, dichloromethane (DCM), ethanol, acetic acid, nitric acid, sodium hydrogen carbonate ($NaHCO_3$), anhydrous magnesium sulphate ($MgSO_4$), hexane, boron tribromide (BBr_3), petroleum ether, 18-crown-6, anhydrous potassium carbonate (K_2CO_3) and toluene were used as received from various reputable suppliers without further purification.

PAF-1 synthesis

PAF-1 was synthesized according to Zhu's work.[23] Briefly, 2,2′-bipyridyl (1.28 g, 8.18 mmol) was added to a stirred solution of degassed bis(1,5-cyclooctadiene)nickel(0) (2.25 g, 8.18 mmol) in anhydrous DMF (120 mL) under argon. 1,5-Cyclooctadiene (1.05 mL, 8.32 mmol) dried over CaH_2 was added under argon and the mixture was heated at 80 °C for 1 h. Tetrakis(4-bromophenyl) methane (1 g, 1.57 mmol) was added under argon atmosphere and the mixture stirred overnight at 80 °C. After cooling to room temperature, HCl/DMF solution (100 mL, 50 : 50 v/v, 37% HCl) was added. The solid was filtered and washed with $CHCl_3$ (8×), THF (8×) and H_2O (8×) and dried under reduced pressure at 100 °C to give PAF-1 as an off-white powder with a surface area 3905 $m^2\ g^{-1}$ (see Fig. S1†). The PAF-1 nanoparticle was characterized in size around 75 ± 10 nm as estimated from SEM images (Fig. 2) and average pore size of 14.4 Å from XRD (Fig. S5a†).

TPIM-2 synthesis

The TPIM-2 synthesis details can be found in our previous work.[20] Briefly, in a Schlenk tube, a mixture of the A-B monomer (1.0 mmol), 18-crown-6 (1.1 mmol), anhydrous DMF (3 mL) and anhydrous K_2CO_3 (3.0 mmol) was stirred at 155 °C for 20 min under nitrogen atmosphere. Followed by the addition of toluene (3 mL), the reaction was continued for another 45 min. Repeat this step by adding more toluene (3 mL). The product was purified by precipitating from methanol and boiling in hot water for 30 min. Yellow-orange powder was dried at reduced pressure at 130 °C for 12 h. The molecular weight (M_w) of TPIM-2 was 86 000 g mol^{-1} and the polydispersity index (M_w/M_n) was 2.33, as determined by gel permeation chromatography (GPC) in chloroform using polystyrene calibration standards.

Membrane fabrication

Briefly, membranes were fabricated by dissolving TPIM-2 powder (200 mg) into chloroform (5 mL). After 24 h stirring and filtration (0.45 μm PTFE cartridge), the solution was then poured into a glass dish and covered with a perforated foil to slowly evaporate the solvent for 48 h. The formed film was dried under vacuum for 12 h at 120 °C to remove residual chloroform. Then, the TPIM-2 film was soaked in methanol for 24 h to remove any trace chloroform, followed by drying under vacuum for 24 h at 120 °C. MMMs were prepared using an identical method except that PAF-1 (10 and 20 mg) was added into the filtrated polymer solution (190 mg and 180 mg) in the fabrication of the TPIM-2@5% PAF-1 and TPIM-2@10% PAF-1 membranes, respectively. The TPIM-2 + PAF-1 solutions were stirred for another 24 h before continuing to casting as the pure polymer film fabrication procedure. TGA (Fig. S2†) did not show any weight loss before 200 °C which indicated that the polymer and MMM films were solvent free and dry before gas permeation testing. All films were placed under reduced pressure overnight to remove any adsorbed residual gas before gas measurements. Sufficient mechanical stability and flexibility of the film samples for gas permeation measurements was confirmed by a simple film folding test (Fig. S3†).

Characterisation

XRD spectra for membranes samples was performed on a Rigaku SmartLab X-ray diffractometer operating under CuKα

radiation (45 kV, 200 mA) with 2θ ranging from 2 to 70° at a step size of 0.04° and scan rate of 2° min^{-1}. XRD spectrum for PAF-1 powder was conducted on a Bruker D8 Advance A25 X-ray diffractometer operating under CuKα radiation (40 kV, 40 mA) with 2θ range of 2 to 85° at a step size of 0.02° and a count time of 1.6 seconds per step. The BET surface area was calculated from N_2 isotherms measured using an ASAP 2420 at 77 K. The sample was activated at 100 °C under vacuum (10^{-6} torr) overnight prior to analysis. Cross-sectional SEM images of membranes were operated on a JEOL JSM-7001 field-emission scanning electron microscope with an accelerating voltage of 5 kV. Viscosity measurements were operated on a SCHOTT AV350 Viscometer (standard ASTM D445) using a 52610/I U-tube calibrated with a de-ionized water standard at 20 °C. Gas permeation measurements were performed on a constant volume/variable pressure gas permeation rig. Further details, including the permeability calculation used are provided in the ESI.† Fourier-transform infrared (FT-IR) spectra for all samples were collected using a Thermo Scientific NICOLET 6700 FT-IR spectrophotometer. Thermal gravimetric analysis (TGA) of membrane was carried out using a Mettler Toledo TGA 2 STAR^e System analyser programmed to heat from 50 to 800 °C at 10 °C min^{-1} under 50 mL min^{-1} nitrogen purge.

Results and discussion

Trade-off

The hydrogen separation performance of pristine TPIM-2 and TPIM-2@PAF-1 mixed-matrix membranes is shown in Fig. 1 together with 2008 and 2015 upper bounds for H_2/CH_4 and H_2/N_2. Consistent with previous work,[20,24] rigid TPIM-2 (as-cast/fresh) films exhibited H_2 permeability of 1651 barrer and H_2/N_2 and H_2/CH_4 selectivities of 19.5 and 16.0, respectively. These properties locate the performance of fresh TPIM-2 slightly above the 2008 Robeson plots for H_2/N_2 and H_2/CH_4.[18]

By incorporating porous PAF-1 (surface area 3905 m^2 g^{-1}, Fig. S1†) into TPIM-2, H_2 permeability improved dramatically with a co-current increase in hydrogen selectivity. TPIM-2@5% PAF-1 and TPIM-2@10% PAF-1 MMMs demonstrated 76% (2907 barrer) and 196% (4886 barrer) higher H_2 permeability than pristine TPIM-2. Hydrogen selectivity also improved with H_2/N_2 selectivity increasing from 19.5 to 27.0 at 5% wt PAF-1 loading. Consequently, these improvements in the TPIM-2@PAF-1 membrane resulted in a permselectivity performance near the 2015 upper bounds for hydrogen gas pairs. We ascribe the gas permeability enhancement to the additional gas transport pathways provided by the porous PAF-1 structure. Increasing the loading of PAF-1 in TPIM-2 from 5 to 10% wt resulted in higher hydrogen permeability. For both membranes, the PAF-1 nanoparticles are homogenously dispersed within the TPIM-2 matrix without any obvious interfacial defects, as shown from cross-section SEM images (Fig. 2).

We hypothesized that the simultaneous increase in permeability and selectivity for the MMM samples was due to PAF-1 providing both additional free volume for faster transport, as well as inducing tighter polymer chain packing to improve the membrane's size sieving effect. This is supported by the WAXD spectra (Fig. 3) with the disappearance of the large *d*-spacing of 17.4 Å from TPIM-2 after addition of PAF-1 for both 5 and 10% wt loadings corresponding to an overall shift in the pore size distribution of the polymer towards a tighter average chain structure. It is interesting to note from Fig. 1 that selectivity increased more for low (5% wt, highlighted by red arrow in Fig. 1) rather than high PAF-1 loading (10% wt, highlighted by blue arrow in Fig. 1). For instance, H_2/N_2 selectivity of 19.5 for pure TPIM-2 increased to 27.0 for TPIM-2@5% PAF-1 and 23.4 for TPIM-2@10% PAF-1. This result can be potentially ascribed to non-selective void formation induced at higher PAF-1 loading clusters, reducing the benefit of including additional filler

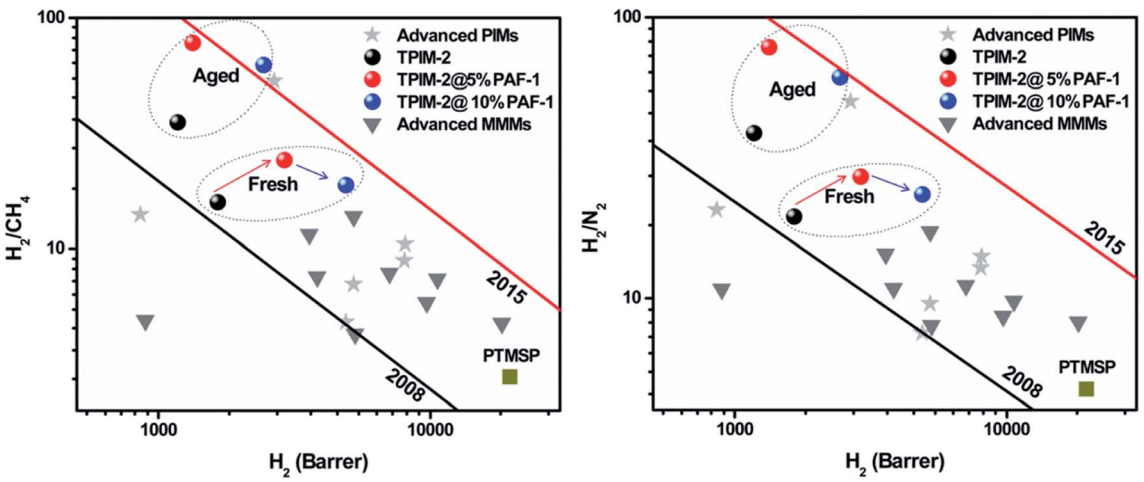

Fig. 1 H_2/CH_4 and H_2/N_2 permeability/selectivity trade-off for TPIM-2-based membranes (as-cast/fresh and aged two months): pristine TPIM-2 (black circle); TPIM-2@5% PAF-1 (red circle); TPIM-2@10% PAF-1 (blue circle) and other PIMs (PTMSP, TPIM-1, PIM-7, PIM-1, PIM-trip-TB, PIM-EA-TB, PIM-SBF) and their MMMs (PIM-1@pDCX, PIM-1@OH-pDCX, PIM-1@PAF-1, PTMSP@PAF-1, PIM-1@UiO-66, PIM-1@Ti_5UiO-66, PIM-1@ZIF-8, PIM-1@silicalite-1, PIM-1@GCNN). Black line: 2008 upper bound. Red line: 2015 upper bound. Red and blue arrows highlighted selectivity change based on PAF-1 loading. Individual data points presented here are summarised in Table S1 of the ESI.†

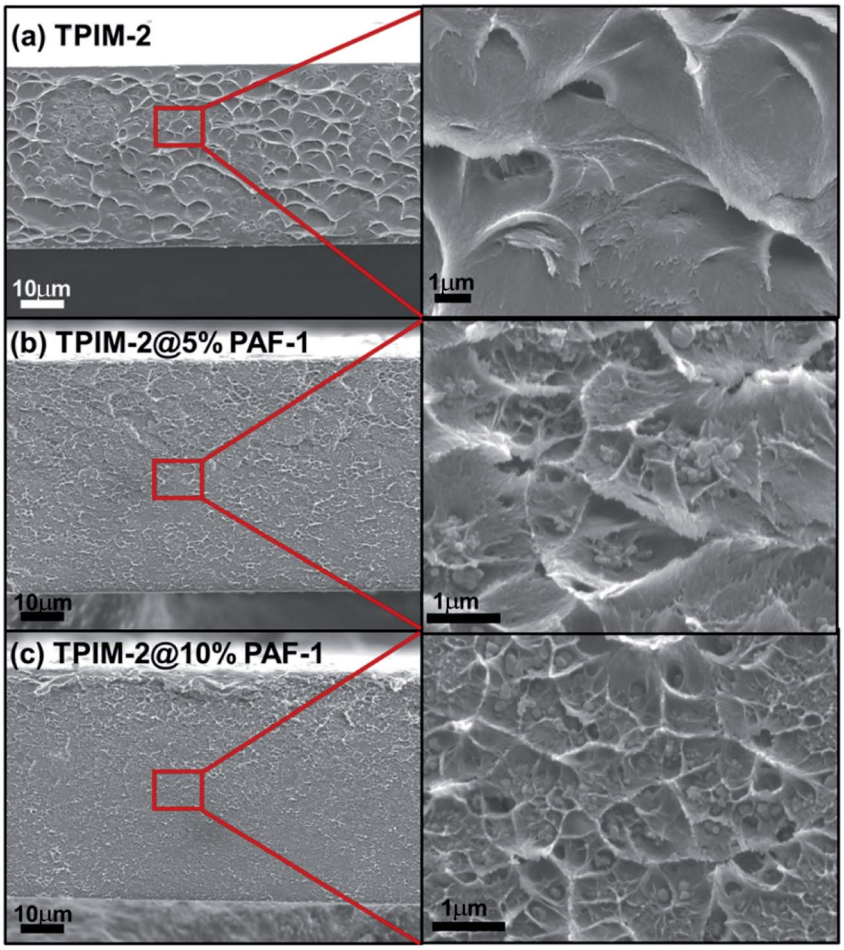

Fig. 2 SEM cross-section for (a) TPIM-2, (b) TPIM-2@5% PAF-1 and (c) TPIM-2@10% PAF-1. Highlighted areas in red frames with 10 μm scale bar were selected for high magnification images with 1 μm scale bar.

material. Similar trends have been previously reported for various MMMs such as PIM-1@SNW-1 for CO_2/N_2,[25] polyoxazoline@Cu-MOF for O_2/N_2,[26] Pebax-1657@4A zeolite for CO_2 separation,[27] and others.[28,29] This is also the reason why we did not attempt to further increase the PAF-1 loading to more than 10% wt as we expected further loss in selectivity as well as mechanical durability.

In Fig. 1, we compare the ideal performance of TPIM-2-based membranes with other fresh and aged pristine PIMs (PTMSP, TPIM-1, PIM-7, PIM-trip-TB, PIM-SBF, PIM-EA-TB and PIM-1) and several of their MMMs (PIM-1/pDCX, PIM-1/OH-pDCX, PIM-1/PAF-1, PTMSP/PAF-1, PIM-1/UiO-66, PIM-1/Ti_5UiO-66, PIM-1/ZIF-8, PIM-1/silicalite-1 and PIM-1/GCNN).[16,20,30–32] As often observed for PIM materials, TPIM-2 and its MMMs displayed an increase in selectivity with a commensurate drop in hydrogen permeability upon aging. For example, a two-months aged TPIM-2@5% PAF-1 sample demonstrated excellent selectivity of 78.0 for both H_2/CH_4 and H_2/N_2. The overall performance of the aged TPIM-2@10% PAF-1 film was significantly improved compared to the fresh sample by reaching the 2015 upper bound for H_2/CH_4 and H_2/N_2 (Fig. 1). The H_2/N_2 selectivity of 61 for TPIM-2@10% PAF-1 aged for 2 months was comparable to that of commercial membrane polymers (*e.g.* $H_2/N_{2(PSF)} = 56$) accompanied with more than two orders of magnitude higher hydrogen permeability ($P(H_2)_{(TPIM\text{-}2@10\%\ PAF\text{-}1\ aged\ 2\ months)} = 2440$ barrer *vs.* $P(H_2)_{(PSF)} = 14.0$ barrer).[10] This result demonstrates the potential of TPIM-2-based MMMs as a promising membrane materials class for hydrogen separation applications.

Physical aging

The long-term performance of each membrane type was investigated by measuring their permeability change over 15, 30, 45, 60, and 180 days for all studied gases (He, H_2, N_2, O_2, CH_4 and CO_2). Normalized permeability loss over time ($P_t/P_{t=0}$) for each membrane is plotted in Fig. 4. The pristine TPIM-2 sample aged for 180 days was not included because the membrane broke during the experiments. As expected, larger gas molecules (N_2 and CH_4) lost permeability over time much faster than smaller gases (He or H_2) for both pristine and MMM samples. This is a general trend among high-free-volume polymers and is responsible for the observed gradual increase in selectivity of light gases over heavy gases selectivity with aging time. For example, we noted that the H_2/CH_4 selectivity of TPIM-2

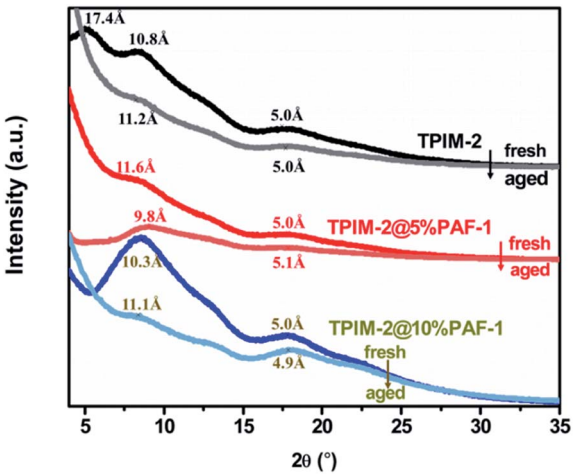

Fig. 3 XRD for fresh and aged TPIM-2, TPIM-2@5% PAF-1 and TPIM-2@10% PAF-1 samples.

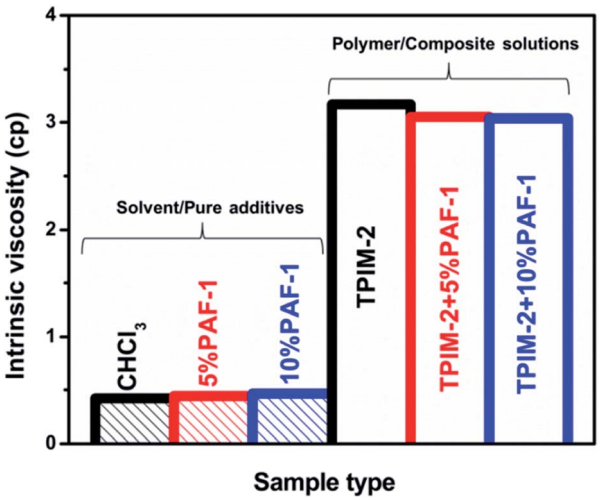

Fig. 5 Viscosity values of TPIM-2 and TPIM-2@PAF-1 in chloroform.

improved from 16.0 to 35.2 after two months aging (Fig. 1 and Table S2†). Interestingly however, this trend was much more pronounced after the inclusion of PAF-1 over the same aging period. Both TPIM-2@PAF-1 MMMs lost more permeability by relative and absolute terms than the pristine TPIM-2 samples (Fig. 4) with TPIM-2@5% PAF-1 losing 54 and 86% and TPIM-2 losing 29 and 68% of their initial H_2 and CH_4 permeabilities, respectively. Although the inclusion of PAF-1 accelerated the time-based permeability loss of the TPIM-2@PAF-1 membranes, the permanent porosity added by PAF-1 into both MMMs meant that they still displayed higher hydrogen permeability (TPIM-2@5% PAF-1 = 1335 barrer and TPIM-2@10% PAF-1 = 2440 barrer) than the pristine TPIM-2 (1175 barrer). As a result of this accelerated aging process, the aged TPIM-2@5% PAF-1 and TPIM-2@10% PAF-1 membrane displayed significantly more favourable hydrogen selectivity of H_2/CH_4 (77.8 and 62.6, respectively) than what is achieved with by the aged pristine TPIM-2 (H_2/CH_4 = 35.2). These results are supported by the observed structural changes revealed by the WAXD spectra for fresh and aged pristine and MMM samples (Fig. 3). Aged pristine TPIM-2 showed main *d*-spacing values of 11.2 and 5.0 Å. Slightly narrower *d*-spacing values were observed for aged TPIM-2@10% PAF-1 (11.1 and 4.9 Å). The aged TPIM-2@5% PAF-1 sample showed a reduction to 9.8 Å for the large *d*-spacing, whereas the smaller one remained at ~5.1 Å. The size-sieving properties of the aged samples follow the relative trend of their reduced *d*-spacing values, that is, as the average *d*-spacing decreased a higher H_2/CH_4 and H_2/N_2 selectivity was obtained.

In 2014, Lau and co-workers reported that the aging process in a series of PIM materials (PIM-1/PMP/PTMSP) could be inhibited by incorporation of PAF-1 nanoparticles, resulting in as little as 5–7% CO_2 permeability loss over 240 days for MMMs compared to 38–62% for the equivalent pure PIMs.[14] In our current work, PAF-1 exhibits the opposite behaviour, seemingly accelerating the physical aging progress for TPIM-2-based MMMs leading to enhanced gas-pair selectivity. Indeed, the high intra-chain rigidity of TPIM-2 (restricted backbone rotations within a chain) did not prevent physical aging, but instead appeared to complement the PAF-1 filler to increase the driving force and kinetics of the aging process.[24] Generally, age-stable membrane properties can be achieved either by further restricting chain dislocations of the membrane matrix polymer

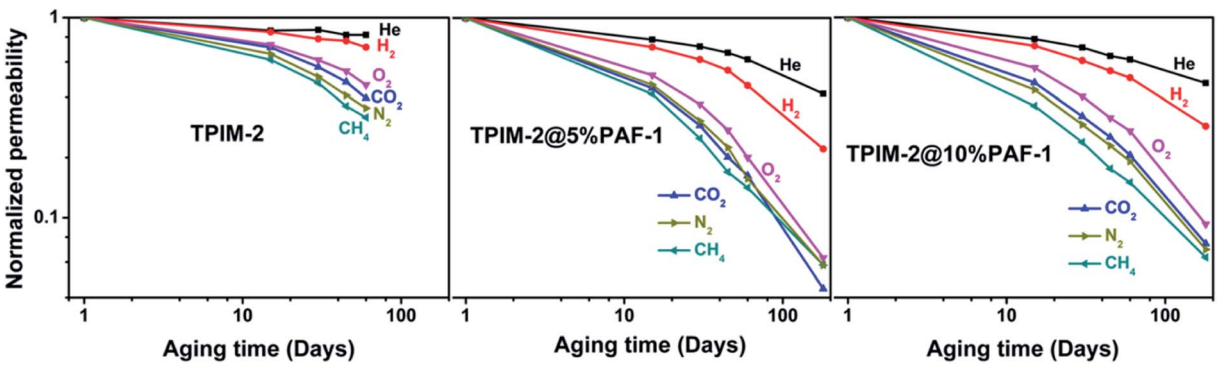

Fig. 4 Normalized permeability ($P_t/P_{t=0}$) of He, H_2, N_2, O_2, CH_4 and CO_2 over time for TPIM-2, TPIM-2@5% PAF-1 and TPIM-2@10% PAF-1. Average permeation data from duplicate. Deviation was within 10%. Each individual data point can be found in ESI Table S2.†

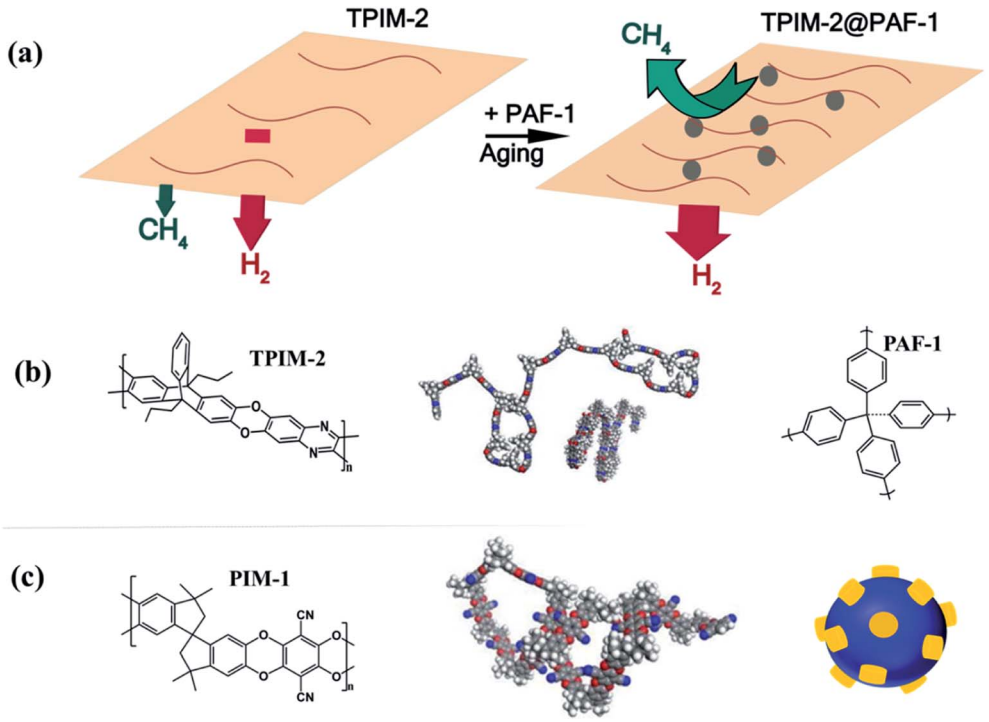

Fig. 6 (a) PAF-1 and aging effect on TPIM-2 polymer rearrangement: both PAF-1 incorporating and aging process encouraged a more densely packed chains state for ribbon-like TPIM-2 polymer, responsible for the significant improved hydrogen selectivities. PAF-1 additive: grey dot. (b) Left: repeat unit of TPIM-2. Middle: TPIM-2 polymer chain conformation. Right: PAF-1 structure. (c) Left: repeat unit of PIM-1. Middle: PIM-1 polymer chain conformation. Right: interaction between PIM-1 (yellow) and PAF-1 (blue): contorted PIM-1 polymer chains partially threaded into pores of PAF-1, responsible for the pronounced slowed PIM-1 aging behaviour. Polymer chain conformation was adapted from ref. 24 with permission from American Chemical Society.

structure through chain–chain interactions or by accelerating the aging process by some means to more quickly approach thermal equilibrium. The mitigated physical aging behaviour in Lau's work[14] can be explained by stabilizing the polymer structure through partial chains intercalation within PAF-1 pores. This effect was further explored in the works of Smith *et al.* which demonstrated that this polymer–additive interaction acted as the key parameter for MMM performance and material properties.[33,34] Adhesive nanoparticles slowed the physical aging densification rate at the polymer and additive boundary of the MMM, whereas nanoparticles that do not deliver an adhesive reaction can speed up localized age-related densification.

Interaction between TPIM-2 and PAF-1

To further understand the different aging behaviour of pristine TPIM-2 and TPIM-2@PAF-1 MMMs, viscosity measurements in chloroform were conducted. As previously reported,[35–37] slowed physical aging in PIM-derived MMMs is often accompanied with a reduction in viscosity with solution mixing time due to a decrease in polymer chain entanglement achieved through either chain adsorption on the additive surface or intrusion into the additive's pores, in addition to the free volume added by the porous filler.

In contrast to the anti-aging behaviour reported by Lau and co-workers,[14,35,36] here the viscosity of pure and composite TPIM-2 casting solutions did not show any obvious change during the 24 h stirring period (Fig. 5). Hence, possible interactions between TPIM-2 and PAF-1 could not be identified through viscosity measurements. We attribute the diverse range of possible molecular interactions between PAF-1 with various PIM polymers is responsible for the different aging of the TPIM-2@PAF-1 and PIM-1@PAF-1 MMM observed.

Infrared spectroscopy did not reveal any differences in chemical bonding or interactions between for the fresh and aged samples (Fig. S4†). Instead the different interactions with PIM materials (TPIM-2 *vs.* PIM-1) might be explained by the different polymer microstructures caused by the included PAF-1 nanoparticles. As proposed in previous work,[24] more efficient hydrogen separation performance was realized through the densely packed ribbon-like (one plane propagation) structure of TPIMs compared to the contorted architecture of PIM-1. A possible reason for this trend could be that TPIM-2 appears to approach its chain packing equilibrium faster. Our results suggest this effect may also be encouraged in MMMs of these polymers that contain additives with certain interactions with the matrix. Here, the inclusion of PAF-1 resulted in a faster aging rate (Fig. 4) and denser polymer chain packing state than the pristine polymer achieves independently (Fig. 3). The different effects of PAF-1 on ribbon-like TPIM-2 and contorted PIM-1 are depicted in Fig. 6.

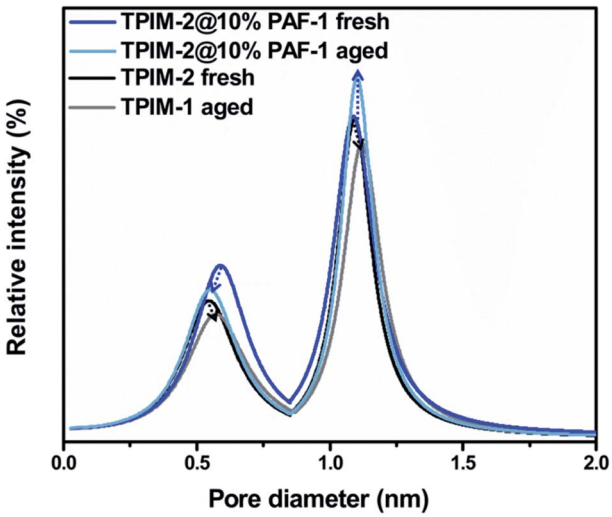

Fig. 7 PALS measurements for fresh and aged TPIM-2 and TPIM-2@10% PAF-1. Dashed arrows: average pore size shift upon aging. Blue dashed arrow: TPIM-2@10% PAF-1 membrane. Black dashed arrow: TPIM-2 membrane.

Positron annihilation lifetime spectroscopy (PALS) was utilized to further elucidate the effect of PAF-1 on TPIM-2. Pristine TPIM-2 and TPIM-2@10% PAF-1 samples were investigated by PALS before and after physical aging (180 days); TPIM-2@5% PAF-1 was excluded from PALS due to insufficient sample mass. According to PALS, TPIM-2 exhibits a bimodal pore size distribution centred at ~5 and ~11 Å, respectively. For the as-cast (fresh) membranes, the intensity of the smaller pore (~5 Å) increased by 24% (+63% fractional free volume, FFV) in the TPIM-2@10% PAF-1 relative to the pristine TPIM-2 (Fig. 7 and Table S3†). By comparison, no changes were observed in the intensity or size (FFV remained) of larger pore (~11 Å) with the addition of PAF-1 to the as-cast membrane. This appears to support the large increase in hydrogen permeability (+196%) and improved selectivity (+20% for H_2/N_2) as selectivity is usually attributed to the smaller pores of a membrane which are more effective size-based sieves. With aging, the decrease in small pore (−11%) and large pore (−18%) intensity for pristine TPIM-2 was matched by a reduction in permeability, and only gradual improvement in selectivity through the slight shift right (to larger values) in pore size distribution. The combinational effect of reduced pores intensity and increased pores size resulted in unaffected total fractional free volume after aging. A similar observation was made for the intensity of the small pore of the TPIM-2@10% PAF-1 membrane, which decreased by 13%. A corresponding reduction in the pore size from 5.9 Å to 5.6 Å results in significantly higher hydrogen selectivity for the aged MMM relative to the pristine TPIM-2 membrane. Contrastingly, the concentration of large pores of the MMM increased by 12% (+15% FFV) with aging. This unusual observation is attributed to presence of the permanent pores of PAF-1 (centred around 14.4 Å, Fig. S5a†) and the proposed influence of the PAF-1 nanoparticles on the polymer microstructure of the aged ribbon-like TPIM-2 polymer matrix.[24] Consequently, we note the high concentration of large pores is likely a cause of higher H_2 permeability of the aged MMM (2440 barrer) relative to the 'less-aged' pristine TPIM-2 (1172 barrer).

Conclusions

Hydrogen, as an environmental-friendly resource and usually existing within Hythane mixture, was separated and purified successfully in this work using membrane technology. Desirable MMMs performance with both high permeability and selectivity was achieved by adding porous PAF-1 into TPIM-2 polymer matrix. Our work demonstrated that hydrogen selectivity (H_2/N_2 = 19.5) of rigid TPIM-2 was enhanced to 27.0 by addition of low loading of porous PAF-1 (5% wt) and further increased to 78.0 over two months aging. Hydrogen permeability of TPIM-2 was improved from 1651 to 4886 barrer by increasing the PAF-1 loading to 10% wt. Upon aging of two months, H_2 permeability of MMMs was ~50% higher (2440 barrer) that the as-cast pristine TPIM-2 membrane. Consequently, both TPIM-2/PAF-1 MMMs displayed performance located on or near the industry attracting area (2015 upper bounds) for H_2/CH_4 and H_2/N_2 separation. The outstanding selectivity enhancement of TPIM-2@PAF-1 MMMs was ascribed to smaller *d*-spacing shift and tighter polymer chain packing with PAF-1 inclusion. Unlike previous work, adhesion of PIM-1 polymer chains to the pore surface of PAF-1 nanoparticles stabilizes the low-density state and initial gas permeability of the membrane. Instead of polymer chains intercalation with PAF-1 and aging mitigation, we found that PAF-1 accelerated the aging process in TPIM-2-based MMMs. Like other studies on PIM polymers that explore the effect polymer structure has on the polymer chain conformation, we note that the two-dimensional propagation/rigid shape of TPIM-2 is a likely reason for the stark difference in aging behaviour (accelerated *vs.* mitigated) compared to other PAF-containing MMMs. Ribbon-like TPIM-2 (one plane propagation) appears to have a greater ability to reach its equilibrium polymer chain packing state compared with the more contorted PIM-1 polymer architecture. With addition of PAF-1, narrowed inter-chains *d*-spacing and densified polymer structure towards suggesting the additive catalysed the structural densification of the MMM's polymer phase and resulted into the accelerated TPIM-2 aging behaviour accompanied with remarkably improved hydrogen selectivity. Combining eminent hydrogen selectivity and with orders of magnitude higher permeability highlights the considerable potential of the presented TPIM-2@10% PAF-1 composite membranes for high performance separation of hydrogen necessary for the emerging hydrogen economy.

Conflicts of interest

The authors declare no competing interests.

Acknowledgements

MCEM facility from Chemical Engineering Department of Monash University, XRD and FT-IR from CSIRO. Polymer

synthesis was supported by baseline funding from King Abdullah University of Science and Technology (BAS/1/1323-01-01). CMD acknowledges the Veski Inspiring Women Fellowship. MRH acknowledges the ARC for support (FT130100345).

References

1 K. Chong, S.-O. Lai, H. S. Thiam, H. C. Teoh and S. Heng, *J. Eng. Sci. Technol.*, 2016, **11**, 1016–1030.
2 M. Galizia, W. S. Chi, Z. P. Smith, T. C. Merkel, R. W. Baker and B. D. Freeman, *Macromolecules*, 2017, **50**, 7809–7843.
3 D. S. Sholl and R. P. Lively, *Nature*, 2016, **532**, 435.
4 P. Bernardo, E. Drioli and G. Golemme, *Ind. Eng. Chem. Res.*, 2009, **48**, 4638–4663.
5 B. Ibeh, C. Gardner and M. Ternan, *Int. J. Hydrogen Energy*, 2007, **32**, 908–914.
6 S. Adhikari and S. Fernando, *Ind. Eng. Chem. Res.*, 2006, **45**, 875–881.
7 N. W. Ockwig and T. M. Nenoff, *Chem. Rev.*, 2007, **107**, 4078–4110.
8 M. Najafi, M. Sadeghi, A. Bolverdi, M. Pourafshari Chenar and M. Pakizeh, *Adv. Polym. Technol.*, 2018, **37**, 2043–2052.
9 R. Castro-Muñoz and V. Fíla, *Membranes*, 2018, **8**, 30.
10 V. Abetz, T. Brinkmann, M. Dijkstra, K. Ebert, D. Fritsch, K. Ohlrogge, D. Paul, K. V. Peinemann, S. Pereira-Nunes, N. Scharnagl and M. Schossig, *Adv. Eng. Mater.*, 2006, **8**, 328–358.
11 P. M. Budd, K. J. Msayib, C. E. Tattershall, B. S. Ghanem, K. J. Reynolds, N. B. McKeown and D. Fritsch, *J. Membr. Sci.*, 2005, **251**, 263–269.
12 P. M. Budd and N. B. McKeown, *Polym. Chem.*, 2010, **1**, 63–68.
13 N. B. McKeown and P. M. Budd, *Chem. Soc. Rev.*, 2006, **35**, 675–683.
14 C. H. Lau, P. T. Nguyen, M. R. Hill, A. W. Thornton, K. Konstas, C. M. Doherty, R. J. Mulder, L. Bourgeois, A. C. Y. Liu, D. J. Sprouster, J. P. Sullivan, T. J. Bastow, A. J. Hill, D. L. Gin and R. D. Noble, *Angew. Chem., Int. Ed.*, 2014, **53**, 5322–5326.
15 H. B. Park, J. Kamcev, L. Robeson, M. Elimelech and B. Freeman, *Science*, 2017, **356**, 1138–1148.
16 R. Hou, S. J. D. Smith, C. D. Wood, R. J. Mulder, C. H. Lau, H. Wang and M. R. Hill, *ACS Appl. Mater. Interfaces*, 2019, **11**, 6502–6511.
17 B. D. Freeman, *Macromolecules*, 1999, **32**, 375–380.
18 L. Robeson, *J. Membr. Sci.*, 2008, **320**, 390–400.
19 R. Swaidan, B. Ghanem and I. Pinnau, *ACS Macro Lett.*, 2015, **4**, 947–951.
20 B. S. Ghanem, R. Swaidan, X. Ma, E. Litwiller and I. Pinnau, *Adv. Mater.*, 2014, **26**, 6696–6700.
21 S. J. D. Smith, R. Hou, C. H. Lau, K. Konstas, M. Kitchin, G. Dong, J. Lee, W. H. Lee, J. G. Seong, Y. M. Lee and M. R. Hill, *J. Membr. Sci.*, 2019, **585**, 260–270.
22 X. Q. Cheng, K. Konstas, C. M. Doherty, C. D. Wood, X. Mulet, Z. Xie, D. Ng, M. R. Hill, C. H. Lau and L. Shao, *ChemSusChem*, 2017, **10**, 1887–1891.
23 T. Ben, H. Ren, S. Ma, D. Cao, J. Lan, X. Jing, W. Wang, J. Xu, F. Deng, J. M. Simmons, S. Qiu and G. Zhu, *Angew. Chem., Int. Ed.*, 2009, **48**, 9457–9460.
24 R. Swaidan, B. Ghanem, E. Litwiller and I. Pinnau, *Macromolecules*, 2015, **48**, 6553–6561.
25 X. Wu, Z. Tian, S. Wang, D. Peng, L. Yang, Y. Wu, Q. Xin, H. Wu and Z. Jiang, *J. Membr. Sci.*, 2017, **528**, 273–283.
26 S. Y. Lim, J. Choi, H.-Y. Kim, Y. Kim, S.-J. Kim, Y. S. Kang and J. Won, *J. Membr. Sci.*, 2014, **467**, 67–72.
27 R. Surya Murali, A. F. Ismail, M. A. Rahman and S. Sridhar, *Sep. Purif. Technol.*, 2014, **129**, 1–8.
28 B. Ghalei, K. Sakurai, Y. Kinoshita, K. Wakimoto, A. P. Isfahani, Q. Song, K. Doitomi, S. Furukawa, H. Hirao, H. Kusuda, S. Kitagawa and E. Sivaniah, *Nat. Energy*, 2017, **2**, 17086.
29 N. Jusoh, Y. F. Yeong, K. K. Lau and A. M. Shariff, *Procedia Eng.*, 2016, **148**, 1259–1265.
30 M. Carta, M. Croad, R. Malpass-evans, J. C. Jansen, P. Bernardo, G. Clarizia, K. Friess, M. Lanč and N. B. McKeown, *Adv. Mater.*, 2014, **26**, 3526–3531.
31 R. Castro-Muñoz, V. Fila and C. Dung, *Chem. Eng. Commun.*, 2017, **204**(3), 295–309.
32 S. J. D. Smith, B. P. Ladewig, A. J. Hill, C. H. Lau and M. R. Hill, *Sci. Rep.*, 2015, **5**, 7823.
33 S. J. D. Smith, C. H. Lau, J. I. Mardel, M. Kitchin, K. Konstas, B. P. Ladewig and M. R. Hill, *J. Mater. Chem. A*, 2016, **4**, 10627–10634.
34 S. J. D. Smith, K. Konstas, C. H. Lau, Y. M. Gozukara, C. D. Easton, R. J. Mulder, B. P. Ladewig and M. R. Hill, *Cryst. Growth Des.*, 2017, **17**, 4384–4392.
35 C. H. Lau, K. Konstas, A. Thornton, A. Liu, S. Mudie, D. Kennedy, S. Howard, A. Hill and M. Hill, *Angew. Chem., Int. Ed. Engl.*, 2015, **54**(9), 2669–2673.
36 C. H. Lau, X. Mulet, K. Konstas, C. M. Doherty, M.-A. Sani, F. Separovic, M. R. Hill and C. D. Wood, *Angew. Chem., Int. Ed.*, 2016, **55**, 1998–2001.
37 S. Jain, J. G. P. Goossens, G. W. M. Peters, M. van Duin and P. J. Lemstra, *Soft Matter*, 2008, **4**, 1848–1854.

